

---

# PHYSICS-INFORMED NEURAL NETWORKS WITH HARD NONLINEAR EQUALITY AND INEQUALITY CONSTRAINTS

---

Ashfaq Iftakher\*  
iftakher@tamu.edu

Rahul Golder\*  
rahulgolder8420@tamu.edu

M. M. Faruque Hasan  
hasan@tamu.edu<sup>‡</sup>

## ABSTRACT

Traditional physics-informed neural networks (PINNs) do not guarantee strict constraint satisfaction. This is problematic in engineering systems where minor violations of governing laws can significantly degrade the reliability and consistency of model predictions. In this work, we develop KKT-Hardnet, a PINN architecture that enforces both linear and nonlinear equality and inequality constraints up to machine precision. It leverages a projection onto the feasible region through solving Karush-Kuhn-Tucker (KKT) conditions of a distance minimization problem. Furthermore, we reformulate the nonlinear KKT conditions using log-exponential transformation to construct a general sparse system with only linear and exponential terms, thereby making the projection differentiable. We apply KKT-Hardnet on both test problems and a real-world chemical process simulation. Compared to multilayer perceptrons and PINNs, KKT-Hardnet achieves higher accuracy and strict constraint satisfaction. This approach allows the integration of domain knowledge into machine learning towards reliable hybrid modeling of complex systems.

**Keywords** Machine Learning · Constrained Learning · Physics-informed neural network · Surrogate modeling

## 1 Introduction

Neural networks have gained widespread popularity as surrogate models that enable fast approximate predictions of complex physical systems. Among them, physics-informed neural networks (PINNs) have emerged as a powerful technique to embed first principles-based physical knowledge directly into the learning process. Unlike purely data-driven models, PINNs integrate known physical constraints into the training objective, typically by augmenting the loss function with penalty terms that account for constraint violations [1]. These constraints may include algebraic equations [2], ordinary and partial differential equations [3, 4, 5], or combinations thereof. Although such high-fidelity models mimic the underlying physics, they are often computationally prohibitive, particularly in practical scenarios, such as real-time control [6] or large-scale optimization [7]. This has motivated the development of models that approximate the input–output behavior of these systems while reducing computational burden [8, 9, 10, 11]. Surrogate models are increasingly deployed in chemical process systems, ranging from thermodynamic property predictions to unit operations and full process flowsheet simulation and optimization [12].

Among various surrogate modeling strategies, symbolic regression tools like ALAMO [13, 14] optimize a linear combination of basis functions using mathematical programming, yielding interpretable functional forms. Artificial Neural networks (ANN) approximate continuous nonlinear functions [15], and have shown exceptional performance across a variety of engineering domains and tasks, including computer vision and language [16, 17, 18, 19], model predictive control [20], transport phenomena [21] and structure–property relationships for complex molecules [22]. However, the black-box nature of ANNs hinders their utility in domains that require physical consistency and interpretability [23]. The unconstrained ANN training often results in predictions that violate known conservation laws, making them unreliable for decision making in safety-critical applications. To mitigate this, PINNs incorporate physical laws, typically as soft constraints, into the loss function. While soft-constrained PINNs are flexible and generalizable, they

---

\*Artie McFerrin Department of Chemical Engineering, Texas A&M University, College Station, TX 77843-3122, USA

†Texas A&M Energy Institute, Texas A&M University, College Station, TX 77843, USA

‡Corresponding author: hasan@tamu.edu

suffer from several drawbacks. First, this multi-objective optimization trades prediction accuracy with physical fidelity, but does not guarantee strict satisfaction of the constraints [24, 5, 25]. Constraint violations (although penalized) can persist, especially when data is scarce or highly nonlinear [26, 27]. This is particularly problematic in process systems engineering applications, where surrogate models are cascaded across interconnected unit operations. Even small constraint violations at the component level can accumulate and propagate, undermining the validity of the full system model [28]. Second, training PINNs is challenging due to the nonconvexity of the objective function landscape induced by soft constraints and the requirement of careful tuning of the penalty parameters [29, 30, 31].

To that end, hard-constrained ANNs that embed strict equality and inequality constraints into the model architecture, have recently gained increasing attention. Enforcing hard physical constraints can help regularize models in low-data regimes and prevent overfitting [32, 33]. Hard constrained machine learning approaches typically fall into two broad categories: *projection-based* methods and *predict-and-complete* methods. Projection methods correct errors due to unconstrained predictions by projecting them onto the feasible region defined by the constraints. This is achieved by solving a distance minimization problem [26, 32]. In contrast, predict-and-complete architectures generate a subset of the outputs and analytically complete the rest using constraint equations [34, 35]. Both methods have demonstrated effectiveness in ensuring feasibility during both training and inference. Several notable frameworks have introduced differentiable optimization layers within ANNs to enforce constraints through the Karush-Kuhn-Tucker (KKT) conditions [36]. OptNet [37] pioneered this idea for quadratic programs, which was later extended to general convex programs with implicit differentiation [38]. These techniques have enabled ANNs to solve constrained optimization problems within the forward pass, allowing gradients to propagate through the solution map. Recent works such as HardNet-Cvx [32], DC3 [35] and ENFORCE [39] have applied several of these ideas to a range of convex and nonlinear problems, leveraging fixed-point solvers and the implicit function theorem to compute gradients. For the special case of linear constraints, closed-form projection layers can be derived analytically, thereby avoiding any iterative schemes to ensure feasibility [4, 26]. While most problems of practical importance are nonlinear, limited work exists to ensure hard nonlinear constraints in ANN outputs. Specifically, enforcing nonlinear equality and inequality constraints, especially those involving exponential, polynomial, multilinear or rational terms in both the input or output remains a challenge. Few recent works, for example, ENFORCE [39], attempted to address the case for nonlinear equality constraints by stacking differentiable projection layers. However, they often require problem-specific tuning, and may not guarantee rapid convergence.

In this work, we introduce a PINN architecture that rigorously enforces hard nonlinear equality and inequality constraints in both input and output variables. To handle general nonlinearities without resorting to arbitrary basis expansions, we employ a symbolic transformation strategy, where nonlinear algebraic expressions are reformulated using a sequence of auxiliary variables, logarithmic transformations, and exponential substitutions. This results in a generalized system of linear and exponential terms only, which we solve using a Newton-type iterative scheme that is embedded as a differentiable projection layer. The projection step ensures that the final output satisfies the original nonlinear constraints, with the unconstrained multilayer perceptron (MLP) prediction serving as the initial guess. Due to the log-exponential transformation, the slack and dual variables for inequality constraints are automatically guaranteed to be nonnegative, thereby eliminating the need for active set-type strategies. We demonstrate the proposed framework on illustrative examples with nonlinear constraints in both inputs and outputs, as well as using a real-world chemical process simulation problem. Our results show that the proposed approach ensures constraint satisfaction within machine precision. Embedding hard constraints improves both prediction fidelity and generalization performance, when compared to unconstrained MLPs and PINNs with soft constraint regularization.

To summarize, the main contributions of this work are as follows:

- We transform general nonlinear equality and inequality constraints into a structure composed of only linear and exponential relations, using log-exponential transformation of nonlinear terms. The transformation allows to isolate all the nonlinearities in a specific linear and exponential forms.
- We develop a neural network architecture, KKT-Hardnet, for hard constrained machine learning. KKT-Hardnet integrates a projection layer onto MLPs to solve the KKT system of a projection problem via Newton-type iterative scheme, thereby ensuring hard constraint satisfaction.
- We modify the inequalities to equalities using slack variables and model the complementarity conditions using smooth Fischer-Burmeister reformulation [40] to avoid non differentiability at origin. The log-exponential transformation ensures nonnegativity of the Lagrange multipliers and slack variables.
- We show that the proposed hard-constrained PINN improves surrogate model fidelity compared to vanilla MLPs and soft-constrained PINNs, for example, in applications involving nonlinear thermodynamic equations and process simulations.

The remainder of this paper is organized as follows. Section 2 presents the log-exponential transformation and the mathematical formulation of the projection mechanism, alongwith the architecture of KKT-Hardnet. Section 3 presents numerical results for a set of illustrative examples, as well as a highly nonlinear process simulation problem for the separation of azeotropic refrigerant mixtures using ionic liquids. Finally, Section 4 provides concluding remarks and directions for future work.

## 2 Methodology

In many physical systems, the relationship between input variables  $\mathbf{x}$  and output variables  $\mathbf{y}$  is partially governed by known conservation laws, such as mass or energy balances. These relationships can often be expressed as linear/nonlinear equality or inequality constraints. To rigorously embed such domain knowledge into learning, we adopt an ANN architecture that guarantees satisfaction of these constraints during both training and inference.

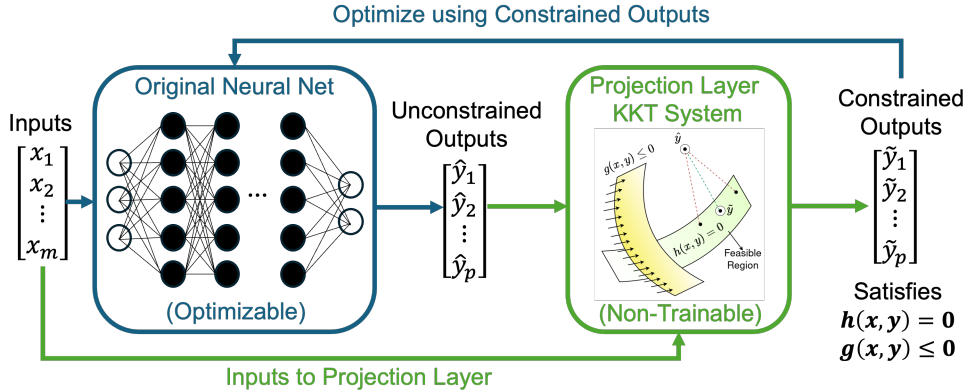


Figure 1: Neural network architecture for hard constrained machine learning (KKT-Hardnet). Unconstrained outputs are calculated using a standard neural net, while the constrained outputs are calculated as the solution of the nonlinear KKT system arising from the physical constraints. The projection layer enforces raw NN output to lie onto the constraint manifold.

Consider a dataset  $\{(\mathbf{x}_i, \mathbf{y}_i)\}_{i=1}^N$  representing the input–output behavior of a physical system. The objective is to train an ANN that approximates the underlying functional mapping between the inputs  $\mathbf{x}$  and the outputs  $\mathbf{y}$ . We consider that some prior knowledge about the system is also available in the form of algebraic constraints that relate the inputs  $\mathbf{x}$  and the outputs  $\mathbf{y}$ . Formally, the goal is to learn  $\mathbf{y} = \text{NN}(\Theta, \mathbf{x})$  such that the predicted outputs  $\mathbf{y}$  always belongs to the feasible set  $\mathcal{S}$ , i.e.,  $\mathbf{y} \in \mathcal{S}$ , where  $\mathcal{S}$  is defined as  $\mathcal{S} = \{\mathbf{y} | \mathbf{h}(\mathbf{x}, \mathbf{y}) = \mathbf{0}, \mathbf{g}(\mathbf{x}, \mathbf{y}) \leq \mathbf{0}\}$ . Specifically,  $\mathbf{h}(\mathbf{x}, \mathbf{y}) = \mathbf{0}$  represents a set of algebraic equality constraints  $h_k(\mathbf{x}, \mathbf{y}) = 0$  for  $k \in \mathcal{N}_E$ , and  $\mathbf{g}(\mathbf{x}, \mathbf{y}) \leq \mathbf{0}$  represents another set of algebraic inequality constraints  $g_k(\mathbf{x}, \mathbf{y}) \leq 0$  for  $k \in \mathcal{N}_I$ . Both the functions  $\mathbf{h}$  and  $\mathbf{g}$  encode domain-specific knowledge, and may be nonlinear in both  $\mathbf{x}$  and  $\mathbf{y}$ . Here, all the aggregated tunable parameters (weights and biases) of an ANN are defined as  $\Theta$ . We make the following assumptions:

1. The number of equality constraints  $\mathcal{N}_E$  is less than or equal to the number of outputs  $p$  of the neural network, i.e.,  $\mathcal{N}_E \leq p$ , to ensure availability of sufficient degrees of freedom for learning from data while satisfying the constraints.
2. The constraint functions  $\mathbf{h}$  are feasible and linearly independent.
3. The inputs are  $\mathbf{x} \in \mathbb{R}^m$  and the outputs are  $\mathbf{y} \in \mathbb{R}_{\geq 0}^p$ .

With these, our approach (see Figure 1) involves augmenting a standard neural network with a *projection layer* (see Figure 2), acting as a corrector. Given an input  $\hat{\mathbf{x}}$ , the network first computes a preliminary output  $\hat{\mathbf{y}}_0 = \text{NN}(\hat{\mathbf{x}})$ , which may violate the physical constraints. The projection layer then adjusts this output to produce a corrected prediction  $\tilde{\mathbf{y}}$  that lies exactly on the constraint manifold. This is achieved by solving a system of nonlinear equations derived from the Karush–Kuhn–Tucker (KKT) conditions associated with the following constrained minimization problem:

$$\begin{aligned} \tilde{\mathbf{y}} = \arg \min_{\mathbf{y}} \quad & \frac{1}{2} \|\mathbf{y} - \hat{\mathbf{y}}_0\|^2 \\ \text{s.t.} \quad & h_k(\mathbf{x}, \mathbf{y}) = 0, \quad \forall k \in \mathcal{N}_E, \\ & g_k(\mathbf{x}, \mathbf{y}) \leq 0, \quad \forall k \in \mathcal{N}_I. \end{aligned} \tag{1}$$

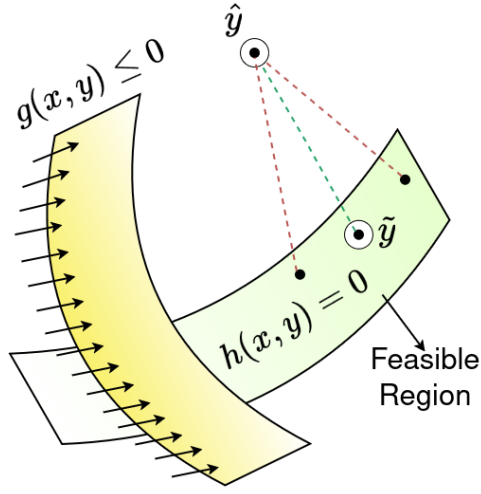


Figure 2: Orthogonal projection of neural net outputs on to the constraint manifold.

This formulation yields an orthogonal projection of the unconstrained prediction  $\hat{\mathbf{y}}_0$  onto the feasible region defined by the constraints in Eq. 1. As we describe later, the solution to the problem in Eq. 1 can be directly embedded in the ANN architecture through enforcing the KKT conditions. The projection step is embedded directly within the forward pass, ensuring that only physically consistent predictions are used for loss computation and backpropagation. As a result, the loss function is modified to:

$$\mathcal{L}_{\text{KKT-Hardnet}} = \frac{1}{2N} \sum_{i=1}^N \|\tilde{\mathbf{y}}_i - \mathbf{y}_i\|^2, \quad (2)$$

in contrast to the conventional loss function used in standard neural networks:

$$\mathcal{L}_{\text{NN}} = \frac{1}{2N} \sum_{i=1}^N \|\hat{\mathbf{y}}_i - \mathbf{y}_i\|^2. \quad (3)$$

Notably, the use of the projected outputs  $\tilde{\mathbf{y}}_i$  alters the learning directions during training, which is informed by the feasible manifold. This ultimately guides the model toward parameters that fit the data while respecting the known constraints. This approach is similar to that of Chen et al. [26] applied to linear equalities; however, we extend it to accommodate both nonlinear equality and inequality constraints. Our framework is architecture-agnostic and can be integrated with any differentiable neural network backbone, including convolutional (CNNs) or recurrent neural networks (RNNs).

To enforce the inequality constraints via KKT Projection, we introduce the non-negative slack variable  $s_k$  for  $k \in \mathcal{N}_I$ , where  $\mathcal{N}_I$  is the number of inequalities, and orthogonally project  $\hat{\mathbf{y}}_0$  onto the feasible set:

$$\begin{aligned} \tilde{\mathbf{y}} &= \arg \min_{\mathbf{y}} \frac{1}{2} \|\mathbf{y} - \hat{\mathbf{y}}_0\|^2 \\ \text{s.t. } & h_k(\mathbf{x}, \mathbf{y}) = 0, \quad \forall k \in \mathcal{N}_E, \\ & g_k(\mathbf{x}, \mathbf{y}) + s_k = 0, \quad \forall k \in \mathcal{N}_I, \\ & s_k \geq 0. \end{aligned} \quad (4)$$

We define the Lagrange multipliers  $\mu_k^E, \mu_k^I \geq 0$ , and write the KKT conditions of the problem in Eq. 4 as follows:

$$\mathbf{y} - \hat{\mathbf{y}}_0 + \sum_{k \in \mathcal{N}_E} \mu_k^E \nabla_{\mathbf{y}} h_k(\mathbf{x}, \mathbf{y}) + \sum_{k \in \mathcal{N}_I} \mu_k^I \nabla_{\mathbf{y}} g_k(\mathbf{x}, \mathbf{y}) = \mathbf{0}, \quad (5)$$

$$\text{(Primal feasibility)} \quad h_k(\mathbf{x}, \mathbf{y}) = 0, \quad k \in \mathcal{N}_E \quad (6)$$

$$\text{(Primal feasibility)} \quad g_k(\mathbf{x}, \mathbf{y}) + s_k = 0, \quad k \in \mathcal{N}_I \quad (7)$$

$$\text{(Dual feasibility)} \quad \mu_k^I \geq 0, \quad s_k \geq 0, \quad k \in \mathcal{N}_I \quad (8)$$

$$\text{(Complementarity)} \quad \phi_k(\mu_k^I, s_k) : \mu_k^I + s_k - \sqrt{(\mu_k^I)^2 + s_k^2} = 0, \quad k \in \mathcal{N}_I. \quad (9)$$

Note that instead of using original complementarity constraint  $\mu_k^I s_k = 0$ , we replace it by the equivalent, smooth Fischer–Burmeister reformulation [40] in Eq. 9. This avoids nondifferentiability at the origin. Furthermore, there exists  $u_k, v_k \in \mathbb{R}$  such that  $\mu_k^I = e^{u_k}$  and  $s_k = e^{v_k}$ . This allows us to apply a log-exp transformation that automatically maintains nonnegativity of the dual and slack variables  $\mu_k^I \geq 0, s_k \geq 0$  during all iterations. Keeping an immediate log-exponential transformation step in mind (more on this is described next) that inherently guarantees the nonnegativity of multipliers and slack variables by construction, we are able to generalize the first-order KKT conditions in a compact form as follows:

$$\begin{aligned} \text{(I)} \quad & \mathbf{y} - \hat{\mathbf{y}}_0 + \nabla_{\mathbf{y}} \tilde{\mathbf{h}}(\mathbf{x}, \mathbf{y})^\top \boldsymbol{\lambda} = 0 \\ \text{(II)} \quad & \tilde{\mathbf{h}}(\mathbf{x}, \mathbf{y}) = \mathbf{0} \end{aligned} \quad (10)$$

where,  $\boldsymbol{\lambda}$  is a vector created by concatenation:  $\boldsymbol{\lambda} = [\boldsymbol{\mu}^E \quad \boldsymbol{\mu}^I \quad \mathbf{s}]$ , and  $\tilde{\mathbf{h}}$  is a vector of functions created by concatenation:  $\tilde{\mathbf{h}} = [\mathbf{h} \quad \mathbf{g} + \mathbf{s} \quad \boldsymbol{\phi}]$ . Therefore,  $\tilde{h}_k = 0$  for  $k \in \mathcal{N}_T$ , where  $\mathcal{N}_T$  is union of the constraints given in Eqs. 6, 7 and 9. This completes the first transformation of the KKT conditions as a system of (nonlinear) equalities.

From here, a natural approach is to enforce these KKT conditions via projection. Before we apply the projection, however, we perform log-exponential transformation of the nonlinear terms to arrive at a generic form of the projection space as described below.

## 2.1 Log-Exponential Transformation

We adopt a symbolic transformation strategy via logarithmic and exponential substitutions. This allows general nonlinear constraints to be rewritten in a structured form where all nonlinearities appear as exponentials and/or linear combinations of variables. Specifically, any constraint of the form  $h(\mathbf{x}, \mathbf{y}) = 0$ , that may include nonlinear terms such  $y^n, xy$ , or  $y/x$  and so on, and can be reformulated into an equivalent system where  $\mathbf{z}$  denotes a set of new auxiliary variables that allows each nonlinear term to be replaced by an exponential. This yields a constraint system of the general form which is equivalent to the system given by Eq. 10:

$$\mathbf{A}\mathbf{x} + \mathbf{B}\mathbf{y} + \mathbf{A}_x \exp(\mathbf{x}) + \mathbf{C}_z \mathbf{z} + \mathbf{C}_\lambda \boldsymbol{\lambda} = \mathbf{b}, \quad (11a)$$

$$\mathbf{D}_y \mathbf{y} + \mathbf{D}_z \mathbf{z} + \mathbf{D}_\lambda \boldsymbol{\lambda} = \mathbf{d}, \quad (11b)$$

$$\mathbf{E}_y \mathbf{y} + \mathbf{E}_z \mathbf{z} + \mathbf{E}_\lambda \boldsymbol{\lambda} = \mathbf{G} \exp(\mathbf{H}_y \mathbf{y} + \mathbf{H}_z \mathbf{z}). \quad (11c)$$

In general, we can denote this new system of equations in Eq. 11 as  $\mathbf{F}(\mathbf{y}, \mathbf{z}, \boldsymbol{\lambda}) = \mathbf{0}$ . The solution of this system of equations gives  $\tilde{\mathbf{y}}$ . Note that, in this transformed general form, all terms are linear except for  $\exp(\mathbf{H}_y \mathbf{y} + \mathbf{H}_z \mathbf{z})$  in Eq. 11c.

To illustrate, consider the nonlinear algebraic constraint:

$$h(\mathbf{x}, \mathbf{y}) := y_1 - y_2^3 - 12x^2 + 6x - 6 = 0. \quad (12)$$

Let  $z_1 := e^{z_5}, z_2 := e^{z_4}, z_3 := y_2^3, z_4 := \log z_3, z_5 := \log y_2$ . This implies  $z_4 = 3z_5, y_2 = e^{z_5}, z_3 = e^{z_4}$ . For inputs, we define:  $x_1 := x, x_2 := x^2, x_3 := \log x_2, x_4 := \log x_1$ , which implies:  $x_3 = 2x_4, x_2 = e^{x_3}, x_1 = e^{x_4}$ .

Using these definitions and auxiliary variables, the original constraint (12) can be rewritten as the following system:

$$y_1 - z_3 - 12x_2 + 6x_1 = 6, \quad (13a)$$

$$x_3 - 2x_4 = 0, \quad (13b)$$

$$x_2 - e^{x_3} = 0, \quad (13c)$$

$$x_1 - e^{x_4} = 0. \quad (13d)$$

$$z_4 - 3z_5 = 0, \quad (13e)$$

$$y_2 - z_1 = 0, \quad (13f)$$

$$z_3 - z_2 = 0, \quad (13g)$$

$$z_1 - e^{z_5} = 0, \quad (13h)$$

$$z_2 - e^{z_4} = 0, \quad (13i)$$

where,  $\mathbf{x} = (x_1, x_2, x_3, x_4)^\top$ ,  $\mathbf{y} = (y_1, y_2)^\top$ , and  $\mathbf{z} = (z_1, \dots, z_5)^\top$ , with:

$$\mathbf{A} = \begin{bmatrix} 6 & -12 & 0 & 0 \\ 0 & 0 & 1 & -2 \\ 0 & 1 & 0 & 0 \\ 1 & 0 & 0 & 0 \end{bmatrix}$$

$$\mathbf{D}_y = \begin{bmatrix} 0 & 0 \\ 0 & 1 \\ 0 & 0 \end{bmatrix}$$

$$\mathbf{B} = \begin{bmatrix} 1 & 0 \\ 0 & 0 \\ 0 & 0 \\ 0 & 0 \end{bmatrix}$$

$$\mathbf{D}_z = \begin{bmatrix} 0 & 0 & 0 & 1 & -3 \\ -1 & 0 & 0 & 0 & 0 \\ 0 & -1 & 1 & 0 & 0 \end{bmatrix}$$

$$\mathbf{A}_x = \begin{bmatrix} 0 & 0 & 0 & 0 \\ 0 & 0 & 0 & 0 \\ 0 & 0 & -1 & 0 \\ 0 & 0 & 0 & -1 \end{bmatrix}$$

$$\mathbf{d} = \begin{bmatrix} 0 \\ 0 \\ 0 \end{bmatrix}$$

$$\mathbf{E}_z = \begin{bmatrix} 1 & 0 & 0 & 0 & 0 \\ 0 & 1 & 0 & 0 & 0 \end{bmatrix}$$

$$\mathbf{C}_z = \begin{bmatrix} 0 & 0 & -1 & 0 & 0 \\ 0 & 0 & 0 & 0 & 0 \\ 0 & 0 & 0 & 0 & 0 \\ 0 & 0 & 0 & 0 & 0 \end{bmatrix}$$

$$\mathbf{H}_z = \begin{bmatrix} 0 & 0 & 0 & 0 & -1 \\ 0 & 0 & 0 & -1 & 0 \end{bmatrix}$$

$$\mathbf{b} = \begin{bmatrix} 6 \\ 0 \\ 0 \\ 0 \end{bmatrix}$$

$$\mathbf{G} = \begin{bmatrix} 1 & 0 \\ 0 & 1 \end{bmatrix}$$

$$\mathbf{H} = \begin{bmatrix} 0 & 0 & 0 & 0 & 1 \\ 0 & 0 & 0 & 1 & 0 \end{bmatrix}$$

, and all other vector and matrices are zero.

This transformation has two major advantages. First, it converts arbitrary nonlinear constraints into a standard structure compatible with Newton-type solvers, where the Jacobian can be easily computed and sparsity can be exploited. Second, it enables rigorous enforcement of nonlinear equality constraints by solving only a system of linear and exponential equations, without the need for arbitrary number of basis functions.

*Remark 1.* We interpret all exponentials component-wise. That is, for any vector  $\mathbf{v}$ ,  $\exp(\mathbf{v}) = [e^{v_1}, e^{v_2}, \dots]^\top$ . In

particular,  $\exp(\mathbf{H}_y \mathbf{y}) = \begin{bmatrix} e^{(\mathbf{H}_y \mathbf{y})_1} \\ e^{(\mathbf{H}_y \mathbf{y})_2} \\ \vdots \end{bmatrix}$ , where each entry is the exponential of the corresponding row of  $\mathbf{H}_y \mathbf{y}$ .

## 2.2 Numerical solution of the general KKT system

As described above, KKT conditions for general linear/nonlinear equality and inequality constraints can be represented as Eq. 11. We employ a projection layer that iteratively solves the nonlinear system of equations corresponding to the KKT system:

$$\mathbf{F}(\mathbf{y}, \mathbf{z}, \boldsymbol{\lambda}) = \begin{pmatrix} F_1(\mathbf{y}, \mathbf{z}, \boldsymbol{\lambda}) \\ F_2(\mathbf{y}, \mathbf{z}, \boldsymbol{\lambda}) \\ F_3(\mathbf{y}, \mathbf{z}, \boldsymbol{\lambda}) \end{pmatrix} = 0$$

where

$$\begin{aligned} F_1(\mathbf{y}, \mathbf{z}, \boldsymbol{\lambda}) &:= \mathbf{A} \hat{\mathbf{x}} + \mathbf{B} \mathbf{y} + \mathbf{A}_x \exp(\hat{\mathbf{x}}) + \mathbf{C}_z \mathbf{z} + \mathbf{C}_\lambda \boldsymbol{\lambda} - \mathbf{b}, \\ F_2(\mathbf{y}, \mathbf{z}, \boldsymbol{\lambda}) &:= \mathbf{D}_y \mathbf{y} + \mathbf{D}_z \mathbf{z} + \mathbf{D}_\lambda \boldsymbol{\lambda} - \mathbf{d}, \\ F_3(\mathbf{y}, \mathbf{z}, \boldsymbol{\lambda}) &:= \mathbf{E}_y \mathbf{y} + \mathbf{E}_z \mathbf{z} + \mathbf{E}_\lambda \boldsymbol{\lambda} - \mathbf{G} \exp(\mathbf{H}_y \mathbf{y} + \mathbf{H}_z \mathbf{z}). \end{aligned} \quad (14)$$

The Jacobian with respect to  $(\mathbf{y}, \mathbf{z}, \boldsymbol{\lambda})$  is

$$\mathbf{J}(\mathbf{y}, \mathbf{z}, \boldsymbol{\lambda}) := \frac{\partial \mathbf{F}}{\partial (\mathbf{y}, \mathbf{z}, \boldsymbol{\lambda})} = \begin{pmatrix} \mathbf{B} & \mathbf{C}_z & \mathbf{C}_\lambda \\ \mathbf{D}_y & \mathbf{D}_z & \mathbf{D}_\lambda \\ \mathbf{E}_y - \mathbf{GLH}_y & \mathbf{E}_z - \mathbf{GLH}_z & \mathbf{E}_\lambda \end{pmatrix}, \quad (15)$$

where

$$\mathbf{L} := \text{diag}(e^{\mathbf{H}_y \mathbf{y} + \mathbf{H}_z \mathbf{z}}).$$

At iteration  $k$ , we solve the (regularized) Newton step

$$[\mathbf{J}(\mathbf{y}^{(k)}, \mathbf{z}^{(k)}, \boldsymbol{\lambda}^{(k)}) + \gamma \mathbf{I}] \begin{pmatrix} \Delta \mathbf{y} \\ \Delta \mathbf{z} \\ \Delta \boldsymbol{\lambda} \end{pmatrix} = -\mathbf{F}(\mathbf{y}^{(k)}, \mathbf{z}^{(k)}, \boldsymbol{\lambda}^{(k)}),$$

and then update

$$\begin{aligned} \mathbf{y}^{(k+1)} &= \mathbf{y}^{(k)} + \alpha \Delta \mathbf{y}, \\ \mathbf{z}^{(k+1)} &= \mathbf{z}^{(k)} + \alpha \Delta \mathbf{z}, \\ \boldsymbol{\lambda}^{(k+1)} &= \boldsymbol{\lambda}^{(k)} + \alpha \Delta \boldsymbol{\lambda}, \end{aligned}$$

where  $\alpha \in (0, 1]$  is a step-length parameter (e.g. from line-search) and  $\gamma > 0$  is a small Tikhonov-regularization constant to ensure invertibility.

---

### Algorithm 1 Newton-KKT projection layer

---

**Require:** Input  $\hat{\mathbf{x}}$ ; unconstrained output  $\hat{\mathbf{y}}_0 = \text{NN}(\hat{\mathbf{x}})$

1: Initialize:  $k \leftarrow 0$ ,  $\mathbf{y}^{(0)} \leftarrow \hat{\mathbf{y}}_0$ ,  $\mathbf{z}^{(0)} \leftarrow \exp(\mathbf{y}^{(0)})$ ,  $\boldsymbol{\lambda} \leftarrow \mathbf{0}$ ,  $\alpha \in (0, 1]$ ,  $\gamma > 0$

2: **repeat**

3:   Compute residual  $\mathbf{F}^{(k)} = \mathbf{F}(\mathbf{y}^{(k)}, \mathbf{z}^{(k)}, \boldsymbol{\lambda}^{(k)})$

4:   Form Jacobian  $\mathbf{J}^{(k)} = \mathbf{J}(\mathbf{y}^{(k)}, \mathbf{z}^{(k)}, \boldsymbol{\lambda}^{(k)})$

5:   Solve Gauss-Newton system:  $[\mathbf{J}^{(k)\top} \mathbf{J}^{(k)} + \gamma \mathbf{I}] \begin{bmatrix} \Delta \mathbf{y} \\ \Delta \mathbf{z} \\ \Delta \boldsymbol{\lambda} \end{bmatrix} = -\mathbf{J}^{(k)\top} \mathbf{F}^{(k)}$

6:   Update:  $\mathbf{y}^{(k+1)} \leftarrow \mathbf{y}^{(k)} + \alpha \Delta \mathbf{y}$ ,  $\mathbf{z}^{(k+1)} \leftarrow \mathbf{z}^{(k)} + \alpha \Delta \mathbf{z}$ ,  $\boldsymbol{\lambda}^{(k+1)} \leftarrow \boldsymbol{\lambda}^{(k)} + \alpha \Delta \boldsymbol{\lambda}$

7:    $k \leftarrow k + 1$

8: **until**  $\|\mathbf{F}^{(k)}\| \leq \varepsilon$  or  $k \geq K$

9: **return**  $\tilde{\mathbf{y}} = \mathbf{y}^{(k)}$ ,  $\tilde{\mathbf{z}} = \mathbf{z}^{(k)}$ ,  $\tilde{\boldsymbol{\lambda}} = \boldsymbol{\lambda}^{(k)}$

---

**Special Case 1: Equality constraints with nonlinearity in  $x$  but linearity in  $y$**

If the equality constraints are affine in  $y$ , then one does not require Newton-type iterative scheme and can derive the projection *analytically* as follows. First, we solve the simplified quadratic program to minimize the euclidean distance between  $\hat{y}_0$  and  $\tilde{y}$  that lies on the constraint manifold.

$$\begin{aligned} \tilde{y} = \arg \min_y \frac{1}{2} \|\mathbf{y} - \hat{y}_0\|^2, \\ \text{s.t. } \mathbf{A}\hat{x} + \mathbf{B}\mathbf{y} + \mathbf{A}_x \exp(\hat{x}) = \mathbf{b}, \end{aligned} \quad (16)$$

The Lagrangian can then be constructed as follows:

$$\mathcal{L}(\mathbf{y}, \boldsymbol{\lambda}) = \frac{1}{2}(\mathbf{y} - \hat{y}_0)^T(\mathbf{y} - \hat{y}_0) + \boldsymbol{\lambda}^\top (\mathbf{A}\hat{x} + \mathbf{B}\mathbf{y} + \mathbf{A}_x \exp(\hat{x}) - \mathbf{b}) \quad (17)$$

Stationary condition:

$$\frac{\partial \mathcal{L}}{\partial \mathbf{y}} = (\mathbf{y} - \hat{y}_0) + \mathbf{B}^T \boldsymbol{\lambda} = 0 \Rightarrow \mathbf{y} = \hat{y}_0 - \mathbf{B}^T \boldsymbol{\lambda} \quad (18)$$

Dual feasibility:

$$\begin{aligned} \frac{\partial \mathcal{L}}{\partial \boldsymbol{\lambda}} &= \mathbf{A}\hat{x} + \mathbf{B}\mathbf{y} + \mathbf{A}_x \exp(\hat{x}) - \mathbf{b} = 0 \\ &\Rightarrow \mathbf{A}\hat{x} + \mathbf{B}(\hat{y}_0 - \mathbf{B}^T \boldsymbol{\lambda}) + \mathbf{A}_x \exp(\hat{x}) - \mathbf{b} = 0 \\ &\Rightarrow \mathbf{A}\hat{x} + \mathbf{B}\hat{y}_0 + \mathbf{A}_x \exp(\hat{x}) - \mathbf{b} = \mathbf{B}\mathbf{B}^T \boldsymbol{\lambda} \end{aligned} \quad (19)$$

If  $\mathbf{B}$  is full rank, then  $\mathbf{B}\mathbf{B}^T$  is invertible.

$$\boldsymbol{\lambda} = (\mathbf{B}\mathbf{B}^T)^{-1} (\mathbf{B}\hat{y}_0 + \mathbf{A}\hat{x} + \mathbf{A}_x \exp(\hat{x}) - \mathbf{b}) \quad (20)$$

$$\begin{aligned} \tilde{y} &= \hat{y}_0 - \mathbf{B}^T (\mathbf{B}\mathbf{B}^T)^{-1} (\mathbf{B}\hat{y}_0 + \mathbf{A}\hat{x} + \mathbf{A}_x \exp(\hat{x}) - \mathbf{b}) \\ &= \left[ \mathbf{I} - \mathbf{B}^T (\mathbf{B}\mathbf{B}^T)^{-1} \mathbf{B} \right] \hat{y}_0 \\ &\quad + \left[ \mathbf{B}^T (\mathbf{B}\mathbf{B}^T)^{-1} \mathbf{A} \right] \hat{x} \\ &\quad + \left[ -\mathbf{B}^T (\mathbf{B}\mathbf{B}^T)^{-1} \mathbf{A}_x \right] \exp(\hat{x}) \\ &\quad + \mathbf{B}^T (\mathbf{B}\mathbf{B}^T)^{-1} \mathbf{b} \\ &= \mathbf{A}^* \hat{x} + \mathbf{B}^* \hat{y}_0 + \mathbf{A}_x^* \exp(\hat{x}) + \mathbf{b}^* \end{aligned} \quad (21)$$

where:

$$\mathbf{A}^* = \mathbf{B}^T (\mathbf{B}\mathbf{B}^T)^{-1} \mathbf{A}, \quad (22a)$$

$$\mathbf{B}^* = \mathbf{I} - \mathbf{B}^T (\mathbf{B}\mathbf{B}^T)^{-1} \mathbf{B}, \quad (22b)$$

$$\mathbf{A}_x^* = -\mathbf{B}^T (\mathbf{B}\mathbf{B}^T)^{-1} \mathbf{A}_x, \quad (22c)$$

$$\mathbf{b}^* = \mathbf{B}^T (\mathbf{B}\mathbf{B}^T)^{-1} \mathbf{b}. \quad (22d)$$

**Special Case 2: Equality constraints with linearity in both  $x$  and  $y$**

Given a linear constraint  $\mathbf{A}\hat{x} + \mathbf{B}\mathbf{y} = \mathbf{b}$ , the projection problem becomes:

$$\tilde{y} = \arg \min_y \frac{1}{2} \|\mathbf{y} - \hat{y}_0\|^2 \quad \text{s.t.} \quad \mathbf{A}\hat{x} + \mathbf{B}\mathbf{y} = \mathbf{b} \quad (23)$$

The solution from KKT conditions is:

$$\tilde{\mathbf{y}} = \hat{\mathbf{y}}_0 - \mathbf{B}^\top (\mathbf{B}\mathbf{B}^\top)^{-1} (\mathbf{B}\hat{\mathbf{y}}_0 + \mathbf{A}\hat{\mathbf{x}} - \mathbf{b}) \quad (24)$$

This can be written in affine form [26]:

$$\tilde{\mathbf{y}} = \mathbf{A}^* \hat{\mathbf{x}} + \mathbf{B}^* \hat{\mathbf{y}}_0 + \mathbf{b}^*, \quad (25)$$

where  $\mathbf{A}^*$ ,  $\mathbf{B}^*$ ,  $\mathbf{b}^*$  are given by Eq. 22a, 22b, and 22d respectively.

To summarize, for constraints involving linear output variables  $\mathbf{y}$ , the KKT conditions allow for an exact, non-iterative projection that can be implemented as a fixed linear layer. However, for general nonlinear constraints defined over both input and output, we resort to Newton-based numerical solution for constraint satisfaction.

### 3 Numerical experiments

We build all machine learning models using the PyTorch package [41]. We use the Adam optimizer [42] for training the models. All numerical experiments are performed on a MacBook Pro with an Apple M4 Pro chip (12-core CPU) and 24 GB of RAM, running macOS. The model implementation and case studies are made available as Jupyter notebook for easy adoption on our GitHub repository at: <https://github.com/aiftakher/KKT-Hardnet>.

#### 3.1 Illustrative example 1: Nonlinearity in both input and output

We consider the scalar input feature  $x \in [1, 2]$  and a nonlinear vector-valued target function

$$\mathbf{y}(x) = \begin{bmatrix} y_1(x) \\ y_2(x) \end{bmatrix} = \begin{bmatrix} 8x^3 + 5 \\ 2x - 1 \end{bmatrix}, \quad \mathbf{y} : \mathbb{R} \rightarrow \mathbb{R}^2. \quad (26)$$

with  $n_{\text{train}} = 1200$  and  $n_{\text{val}} = 300$ . In addition to data  $\{(x_i, \mathbf{y}(x_i))\}_{i=1}^n$ , we assume knowledge of the following algebraic constraint:

$$h(x, \mathbf{y}) := y_1 - y_2^3 - 12x^2 + 6x - 6 = 0. \quad (27)$$

The lagrangian of the following problem becomes:

$$\mathcal{L}(y_1, y_2, \lambda) = \frac{1}{2}(y_1 - \hat{y}_{1,0})^2 + \frac{1}{2}(y_2 - \hat{y}_{2,0})^2 + \lambda h(x, y) \quad (28a)$$

The KKT system becomes:

$$\frac{\partial \mathcal{L}}{\partial y_1} : y_1 - \hat{y}_{1,0} + \lambda = 0, \quad (29a)$$

$$\frac{\partial \mathcal{L}}{\partial y_2} : y_2 - \hat{y}_{2,0} - 3\lambda y_2^2 = 0, \quad (29b)$$

$$\frac{\partial \mathcal{L}}{\partial \lambda} : y_1 - y_2^3 - 12x^2 + 6x - 6 = 0. \quad (29c)$$

Following the definitions and log-exponential transformations in Section 2.1, the KKT system becomes:

$$y_1 - \hat{y}_{1,0} + \lambda = 0, \quad (30a)$$

$$y_2 - \hat{y}_{2,0} - 3z_1 = 0, \quad (30b)$$

$$y_1 - z_2 - 12x_2 + 6x_1 - 6 = 0, \quad (30c)$$

$$z_3 + 2z_4 - z_5 = 0, \quad (30d)$$

$$3z_4 - z_6 = 0, \quad (30e)$$

$$2x_3 - x_4 = 0, \quad (30f)$$

$$\lambda - e^{z_3} = 0, \quad (30g)$$

$$y_2 - e^{z_4} = 0, \quad (30h)$$

$$z_1 - e^{z_5} = 0, \quad (30i)$$

$$z_2 - e^{z_6} = 0, \quad (30j)$$

$$x_1 - e^{x_3} = 0, \quad (30k)$$

$$x_2 - e^{x_4} = 0 \quad (30l)$$

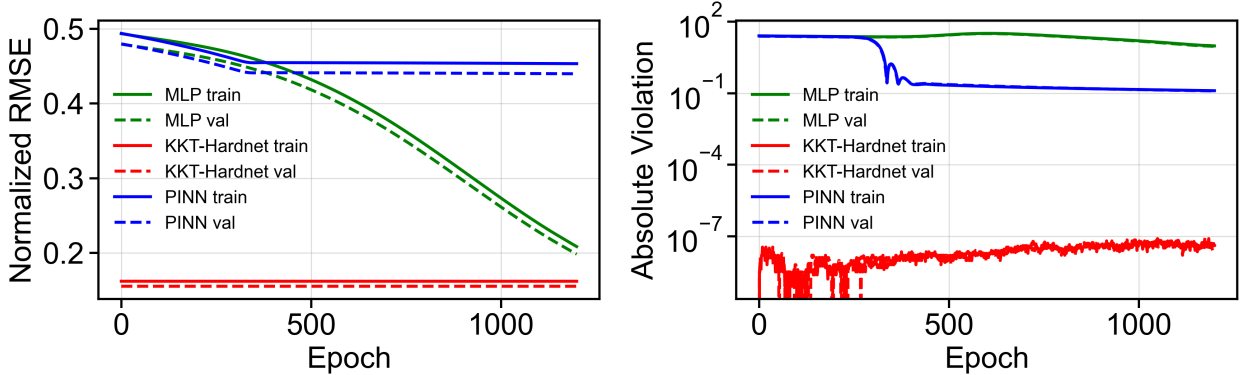


Figure 3: Learning curve of the illustrative example. Left: Normalised RMSE, Right: constraint violation over 1200 epochs.

where,  $\hat{y}_{1,0}$  and  $\hat{y}_{2,0}$  are unconstrained neural net predictions.

Next, we apply Algorithm 1 to seek the closest point on the manifold constructed by equalities in (30). We specify thirty Newton steps ( $K = 30$ ) with tolerance  $\|\mathbf{F}\|_\infty < 10^{-10}$  to reach machine precision. The projector  $\mathcal{P}_s(x, \hat{\mathbf{y}}_0) = (\tilde{\mathbf{y}}_1^{(K)}, \tilde{\mathbf{y}}_2^{(K)})$  is fully differentiable, enabling end-to-end training. We compare three different strategies for handling algebraic constraints: (i) an unconstrained multilayer perceptron (MLP), (ii) a soft physics-informed neural network (PINN), and (iii) our constrained neural network with an embedded Newton projection layer that solves the entire KKT system (KKT-Hardnet). Vanilla MLP involves three hidden layers  $[1 \rightarrow 64 \rightarrow 64 \rightarrow 2]$  with ReLU activation function. The loss function for the training is the mean squared error (MSE). KKT-Hardnet consists of the same backbone as the MLP, followed by the Newton-KKT projection layer. For PINN, with an identical backbone to MLP, the loss is augmented by a soft penalty  $\mathcal{L} = \text{MSE} + \omega(y_1 - y_3 - 12x^2 + 6x - 6)^2$ . All models are trained with Adam ( $\text{lr} = 10^{-4}$ ) for 1200 epochs. The PINN uses penalty weight  $\omega = 100$ .

Figure 3 shows the learning curves for normalized RMSE and absolute constraint violation. The KKT-Hardnet converges nearly an order of magnitude faster and enforces the constraint down to numerical precision, whereas the PINN only reduces the violation to  $\mathcal{O}(10^{-1})$  despite the large penalty weight. Table 1 summarizes performance on both training and validation data. KKT-Hardnet reduces constraint violation by 7–8 orders of magnitude while maintaining lower MSE than the unconstrained baseline. In contrast, PINN incurs large MSE errors due to the difficulty of soft constraint enforcement. Embedding the constraint via a hard Newton projection (KKT-Hardnet) preserves physical consistency exactly while improving regression accuracy. Soft PINN penalties may fail to enforce equality constraint satisfaction unless careful tuning of  $\omega$  is performed.

Table 1: Regression accuracy and constraint violation of KKT-Hardnet compared with an MLP and soft-constrained PINN. MSE values are scaled by the output range.

Model	Training			Validation		
	MSE	MAPE	$ h $	MSE	MAPE	$ h $
MLP	$1.361 \times 10^2$	$2.585 \times 10^{-1}$	9.61	$1.235 \times 10^2$	$2.630 \times 10^{-1}$	9.13
PINN	$6.445 \times 10^2$	$1.664 \times 10^0$	$1.27 \times 10^{-1}$	$6.066 \times 10^2$	$1.672 \times 10^0$	$1.24 \times 10^{-1}$
KKT-Hardnet	$8.253 \times 10^1$	$6.167 \times 10^{-1}$	$4.21 \times 10^{-8}$	$7.585 \times 10^1$	$6.134 \times 10^{-1}$	$3.50 \times 10^{-8}$

### 3.2 Illustrative example 2: Nonlinearity in input only

We consider a two-dimensional input  $\mathbf{x} = (x_1, x_2) \in [1, 2]^2$ , and define a vector-valued ground truth function  $\mathbf{y}(\mathbf{x}) = (y_1(\mathbf{x}), y_2(\mathbf{x}))^\top$  as:

$$\mathbf{y}(x_1, x_2) = \begin{bmatrix} x_1^2 + x_2^2 \\ 4x_1^2 + 4x_2^3 - 2x_2^2 \end{bmatrix}, \quad \mathbf{y} : \mathbb{R}^2 \rightarrow \mathbb{R}^2. \quad (31)$$

We assume the following constraint holds:

$$y_1 + \frac{1}{2}y_2 = 3x_1^2 + 2x_2^3. \quad (32)$$

We then introduce auxiliary variables:

$$x_3 = x_1^2, \quad x_4 = \log x_1, \quad x_5 = \log x_3, \quad (33a)$$

$$x_6 = x_2^3, \quad x_7 = \log x_2, \quad x_8 = \log x_6. \quad (33b)$$

This gives the following augmented system:

$$y_1 + \frac{1}{2}y_2 - 3x_3 - 2x_6 = 0, \quad (34a)$$

$$2x_4 - x_5 = 0, \quad (34b)$$

$$3x_7 = x_8 = 0, \quad (34c)$$

$$x_1 - e^{x_4} = 0, \quad (34d)$$

$$x_3 - e^{x_5} = 0, \quad (34e)$$

$$x_2 - e^{x_7} = 0, \quad (34f)$$

$$x_6 - e^{x_8} = 0. \quad (34g)$$

We collect all eight inputs as  $\mathbf{x} = (x_1, \dots, x_8)^\top \in \mathbb{R}^8$ , and express the constraint system in the general form (see Eq. 11a) as follows:

$$\mathbf{A} = \begin{bmatrix} 0 & 0 & -3 & 0 & 0 & -2 & 0 & 0 \\ 0 & 0 & 0 & 2 & -1 & 0 & 0 & 0 \\ 0 & 0 & 0 & 0 & 0 & 0 & 3 & -1 \\ 1 & 0 & 0 & 0 & 0 & 0 & 0 & 0 \\ 0 & 0 & 1 & 0 & 0 & 0 & 0 & 0 \\ 0 & 1 & 0 & 0 & 0 & 0 & 0 & 0 \\ 0 & 0 & 0 & 0 & 0 & 1 & 0 & 0 \end{bmatrix}, \quad \mathbf{B} = \begin{bmatrix} 1 & \frac{1}{2} \\ 0 & 0 \\ 0 & 0 \\ 0 & 0 \\ 0 & 0 \\ 0 & 0 \\ 0 & 0 \end{bmatrix}, \quad \mathbf{A}_{\mathbf{x}} = \begin{bmatrix} 0 & 0 & 0 & 0 & 0 & 0 & 0 & 0 \\ 0 & 0 & 0 & 0 & 0 & 0 & 0 & 0 \\ 0 & 0 & 0 & 0 & 0 & 0 & 0 & 0 \\ 0 & 0 & 0 & -1 & 0 & 0 & 0 & 0 \\ 0 & 0 & 0 & 0 & -1 & 0 & 0 & 0 \\ 0 & 0 & 0 & 0 & 0 & 0 & -1 & 0 \\ 0 & 0 & 0 & 0 & 0 & 0 & 0 & -1 \end{bmatrix}.$$

**Analytic Projection:** We notice that, only the first row of  $\mathbf{B}$  depends on the output, corresponding to:

$$\mathbf{B}_{\text{active}} \mathbf{y} = 3x_3 + 2x_6, \quad \text{with } \mathbf{B}_{\text{active}} = \begin{bmatrix} 1 & \frac{1}{2} \end{bmatrix}.$$

Rows 2 to 7 do not depend on  $\mathbf{y}$ . Therefore, for any given input  $x_1, x_2$ , all terms in rows 2 to 7 are already satisfied, and thus, they do not participate in the projection. The projection of an unconstrained neural net prediction  $\hat{\mathbf{y}}_0$  onto this hyperplane is therefore, given by the analytic form:

$$\tilde{\mathbf{y}} = \hat{\mathbf{y}}_0 - \mathbf{B}_{\text{active}}^\top \left( \mathbf{B}_{\text{active}} \mathbf{B}_{\text{active}}^\top \right)^{-1} \left( \mathbf{B}_{\text{active}} \hat{\mathbf{y}}_0 - 3x_3 - 2x_6 \right). \quad (35)$$

Since  $\mathbf{B}_{\text{active}} \mathbf{B}_{\text{active}}^\top = \frac{5}{4}$ , the scalar residual  $r$  can be defined as:

$$r = \left( \mathbf{B}_{\text{active}} \hat{\mathbf{y}}_0 - 3x_3 - 2x_6 \right) = \hat{y}_{0,1} + 0.5 \hat{y}_{0,2} - 3x_3 - 2x_6, \quad \text{and} \quad \left( \mathbf{B}_{\text{active}} \mathbf{B}_{\text{active}}^\top \right)^{-1} = \frac{4}{5}.$$

The final projection update becomes:

$$\tilde{\mathbf{y}} = \hat{\mathbf{y}}_0 - \frac{4}{5} \begin{bmatrix} 1 \\ \frac{1}{2} \end{bmatrix} r. \quad (36)$$

$$\boxed{\tilde{y}_1 = \hat{y}_{0,1} - 0.8r, \quad \tilde{y}_2 = \hat{y}_{0,2} - 0.4r.} \quad (37)$$

Note that, if one wishes to consider the entire  $\mathbf{B} \in \mathbb{R}^{7 \times 2}$ , the analytic projection does not change, except  $\mathbf{B}\mathbf{B}^\top$  becomes singular. In that case, one needs to replace the regular inverse with a Moore–Penrose pseudo-inverse [43]. The general projection formula collapses exactly to the same update as given in Eq. 37, because all the zero rows in  $\mathbf{B}$  drop out of the pseudoinverse calculation.

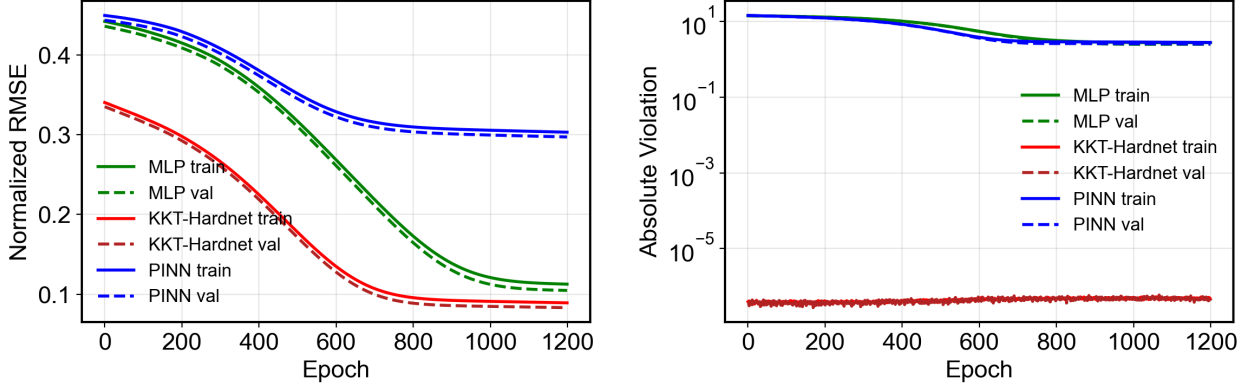


Figure 4: Learning curves for Case 2. Left: Normalized RMSE; Right: absolute constraint violation over 1200 epochs.

**Training results:** We train three models using identical MLP architectures (1-64-64-2) with ReLU activations and the Adam optimizer ( $\text{lr} = 10^{-4}$ , 1200 epochs). Model 1 is MLP which is an unconstrained neural network trained via MSE loss, Model 2 is PINN where MSE loss with soft penalty  $\omega(y_1 + 0.5y_2 - (3x_1^2 + 2x_2^3))$ ,  $\omega = 100$  is applied. Finally, Model 3 is KKT-Hardnet where analytic projection, i.e., Eq. 37, is applied after raw prediction from the MLP backbone. As shown in Figure 4 and Table 2, KKT-Hardnet reduces constraint violation by over 6 orders of magnitude while achieving the lowest validation error. In contrast, the soft-penalty PINN model suffers from large errors due to inadequate constraint enforcement.

Table 2: Regression accuracy and constraint enforcement comparison for the illustrative example 2. RMSE values are unnormalized.

Model	Training			Validation		
	MSE	MAPE	$ h $	MSE	MAPE	$ h $
MLP	$1.443 \times 10^1$	21.0%	2.77	$1.248 \times 10^1$	19.2%	2.51
PINN	$1.045 \times 10^2$	97.9%	2.81	$1.004 \times 10^2$	97.8%	2.55
KKT-Hardnet	$9.051 \times 10^0$	28.9%	$4.60 \times 10^{-7}$	$7.863 \times 10^0$	26.6%	$4.23 \times 10^{-7}$

### 3.3 Illustrative Example 3: Inequality constraints

We demonstrate the general method for hard enforcement of inequality with the task of learning  $y = x^2$  subject to the scalar inequality  $y - x \leq 0$ . We generate data by uniformly sampling  $x$  such that,

$$x_i \sim \mathcal{U}(1, 2), \quad y_i = x_i^2, \quad \begin{cases} i = 1, \dots, 1200 & \text{(training data)} \\ i = 1201, \dots, 1500 & \text{(validation data)} \end{cases} \quad (38)$$

We fit a vanilla MLP  $\hat{y}_0 = \text{NN}_{\Theta}(x) \in \mathbb{R}$  and then project  $\hat{y}_0$  onto  $\{y \mid y \leq x\}$  by performing the following projection:

$$\min_y \frac{1}{2}(y - \hat{y}_0)^2 \quad (39)$$

$$\text{s.t. } y - x + s = 0, \quad (40)$$

$$s \geq 0 \quad (41)$$

The KKT system is then derived as follows:

$$y - \hat{y}_0 + \mu^E = 0, \quad (42)$$

$$\mu^E - \mu^I = 0, \quad (43)$$

$$y - x + s = 0, \quad (44)$$

$$\mu^I s = 0, \quad (45)$$

$$\mu^I \geq 0, \quad (46)$$

$$s \geq 0 \quad (47)$$

Next, we define the following auxiliary variables for the log-exp reformulation:

$$z_3 = \log(\mu), \quad z_5 = \log(s), \quad (48a)$$

$$z_1 = \mu^{I^2}, \quad z_2 = s^2, \quad (48b)$$

$$z_7 = z_1 + z_2, \quad z_4 = 2 z_3, \quad (48c)$$

$$z_6 = 2 z_5, \quad z_{10} = \log(z_7), \quad (48d)$$

$$z_9 = \frac{1}{2} z_{10}, \quad z_8 = e^{z_9}. \quad (48e)$$

These auxiliary variables during log-exp reformulation ensure that at initialization, all logarithmic and exponential relations hold exactly, and that  $\mu^I > 0$ ,  $s > 0$  throughout the Newton iterations. At the start of each forward pass we set

$$y = \hat{y}_0, \quad \mu^E = 0, \quad (49a)$$

$$\mu^I = \text{ReLU}(\hat{y}_0 - x) + \epsilon, \quad (49b)$$

$$s = \text{ReLU}(x - \hat{y}_0) + \epsilon. \quad (49c)$$

with  $\epsilon = 10^{-3}$ .

After the reformulation, the KKT system becomes

$$F_1(\boldsymbol{\tau}) : y - \hat{y}_0 + \mu^E = 0, \quad (50a)$$

$$F_2(\boldsymbol{\tau}) : \mu^E - \mu^I = 0, \quad (50b)$$

$$F_3(\boldsymbol{\tau}) : y - x + s = 0, \quad (50c)$$

$$F_4(\boldsymbol{\tau}) : z_8 - \mu^I - s = 0, \quad (50d)$$

$$F_5(\boldsymbol{\tau}) : \mu^I - e^{z_3} = 0, \quad (50e)$$

$$F_6(\boldsymbol{\tau}) : z_1 - e^{z_4} = 0, \quad (50f)$$

$$F_7(\boldsymbol{\tau}) : 2 z_3 - z_4 = 0, \quad (50g)$$

$$F_8(\boldsymbol{\tau}) : s - e^{z_5} = 0, \quad (50h)$$

$$F_9(\boldsymbol{\tau}) : z_2 - e^{z_6} = 0, \quad (50i)$$

$$F_{10}(\boldsymbol{\tau}) : 2 z_5 - z_6 = 0, \quad (50j)$$

$$F_{11}(\boldsymbol{\tau}) : z_7 - z_1 - z_2 = 0, \quad (50k)$$

$$F_{12}(\boldsymbol{\tau}) : z_9 - \frac{1}{2} z_{10} = 0, \quad (50l)$$

$$F_{13}(\boldsymbol{\tau}) : z_8 - e^{z_9} = 0, \quad (50m)$$

$$F_{14}(\boldsymbol{\tau}) : z_7 - e^{z_{10}} = 0. \quad (50n)$$

where all the variables are compactly represented by a vector  $\boldsymbol{\tau} = [\mathbf{y}, \mathbf{z}, \boldsymbol{\lambda}]$  as follows:

$$\boldsymbol{\tau} = [y, s, \mu^I, \mu^E, z_3, z_5, z_1, z_2, z_7, z_4, z_6, z_8, z_9, z_{10}]^\top$$

These residuals are solved by a damped Gauss–Newton iteration to machine precision tolerance, yielding the projected output  $\tilde{y} = y$  (see Algorithm 1).

**Model training and comparison.** We compare the projection-based constrained neural network (KKT-Hardnet) with an unconstrained MLP and a soft-constrained PINN, all using identical architectures and training routines. Figure 5

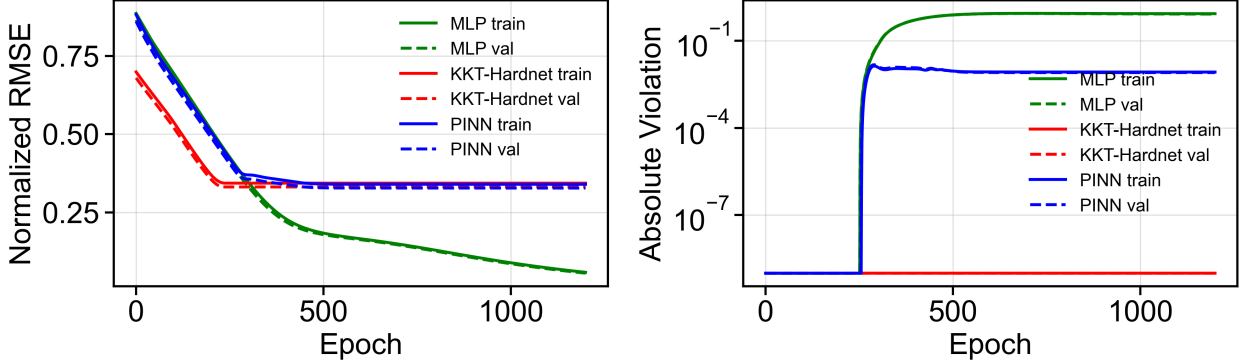


Figure 5: Learning curves for the analytic projection case. Left: Normalized RMSE; Right: absolute constraint violation (log scale).

shows the normalized RMSE and absolute constraint violation for all three models. The results in Table 3 clearly show that KKT-Hardnet maintains constraint satisfaction up to numerical precision while achieving comparable MSE and MAPE to the unconstrained MLP. In contrast, the PINN suffers from persistent constraint violations despite soft penalty enforcement.

Table 3: Model performance with analytic projection for output-only linear constraints.

Model	Training			Validation		
	MSE	MAPE	$ g $	MSE	MAPE	$ g $
MLP	$3.038 \times 10^{-2}$	$7.269 \times 10^{-2}$	$8.48 \times 10^{-1}$	$2.767 \times 10^{-2}$	$7.401 \times 10^{-2}$	$8.22 \times 10^{-1}$
PINN	$1.037 \times 10^0$	$3.035 \times 10^{-1}$	$8.32 \times 10^{-3}$	$9.648 \times 10^{-1}$	$2.948 \times 10^{-1}$	$8.00 \times 10^{-3}$
KKT-Hardnet	$1.059 \times 10^0$	$3.068 \times 10^{-1}$	$1.00 \times 10^{-9}$	$9.857 \times 10^{-1}$	$2.979 \times 10^{-1}$	$1.00 \times 10^{-9}$

### 3.4 Case study: Extractive distillation for azeotropic refrigerant separation

We consider the simulation of an extractive distillation process for separating the azeotropic refrigerant mixture R-410A using the ionic liquid [EMIM][SCN]. The flowsheet is given in Figure 6, which consists of a distillation column with an ionic liquid entrainer fed at a fixed column stage. The feed R-410A is an azeotropic mixture of R-32 and R-125. Therefore, the mass composition of R-32 and R-125 in R-410A feed are 0.5 and 0.5, respectively. [EMIM][SCN] and R-410A are assumed to be fed at stage 2 and 11 respectively. The total number of stages of the columns is set to 18. Due to the presence of ionic liquids as entrainer, highly nonlinear thermodynamics is present for the calculation of phase equilibria across the extractive distillation column. In this case study, all simulations are performed using equilibrium-stage modeling using NRTL model in Aspen Plus<sup>®</sup> v12. Details can be found elsewhere [22, 2, 44].

#### 3.4.1 Problem setup and data generation

We vary three input variables: total feed molar flow rate ( $F_F$ ), ionic liquid flow rate ( $F_{IL}$ ), and the reflux ratio ( $R$ ), and extract a set of steady-state outputs from Aspen Plus. The input space is sampled on a uniform grid: (1) Feed flow rate:  $F_F \in [95, 110]$  kg/hr, (2) IL flow rate:  $F_{IL} \in [800, 950]$  kg/hr, and (3) Reflux ratio:  $R \in [2.5, 4.3]$ . The corresponding outputs include: (1) Distillate and bottoms flowrates:  $F_D, F_B$  [mol/s], (2) Tray liquid flowrate:  $L$  [mol/s], (3) Mole fractions in distillate and bottoms:  $x_{R32}^D, x_{R125}^D, x_{IL}^D, x_{R32}^B, x_{R125}^B, x_{IL}^B$ . Not all simulations converged without error. Therefore, we postprocessed all simulations, and filtered out unconverged ones. This resulted in 4308 simulation data points, which constitute our dataset.

#### 3.4.2 Nonlinear constraints in both input and output

We consider six physical constraints, derived from mass and energy balances involving mixed linearity and nonlinearities in both inputs and outputs:

(C1) Overall molar balance (affine):

$$F_F + F_{IL} = F_D + F_B \quad (51)$$

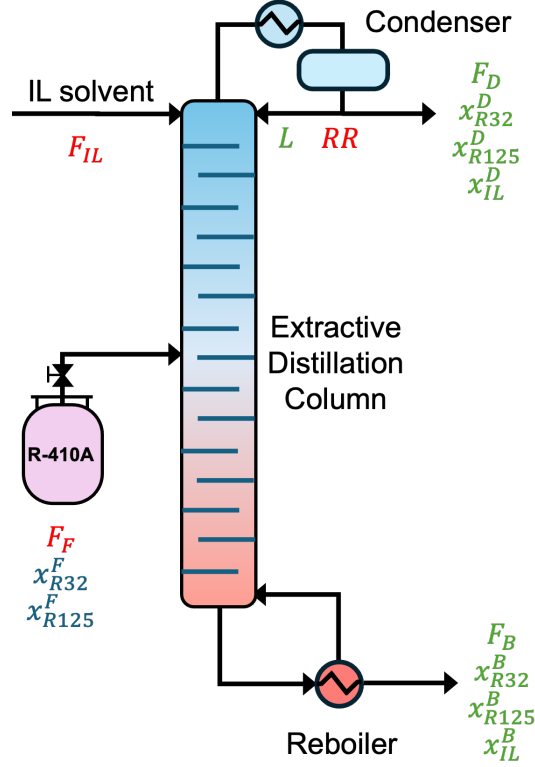


Figure 6: Extractive distillation of R-410A using an Ionic liquid [EMIM][SCN]. The input variables are denoted in red. The output variables are denoted in green. The fixed parameters are denoted in blue. The column operates at a fixed pressure of 10 bar.

(C2) Component balance – R32 (nonlinear in input-output):

$$F_F x_{R32}^F = F_D x_{R32}^D + F_B x_{R32}^B \quad (52)$$

(C3) Component balance – R125 (nonlinear in input-output):

$$F_F x_{R125}^F = F_D x_{R125}^D + F_B x_{R125}^B \quad (53)$$

(C4) Mole fraction balance – Distillate (affine):

$$x_{R32}^D + x_{R125}^D + x_{IL}^D = 1 \quad (54)$$

(C5) Mole fraction closure – Bottoms (affine):

$$x_{R32}^B + x_{R125}^B + x_{IL}^B = 1 \quad (55)$$

(C6) Reflux ratio relation (bilinear in input and output):

$$R = \frac{L}{F_D} \quad (56)$$

Here,  $x_{R32}^F = 0.697616946$  and  $x_{R125}^F = 0.302383054$ .

Next, we enforce the six nonlinear algebraic constraints by constructing the KKT system and log-exponential transformation (see Section 2.1 for details). Specifically, bilinear terms like  $F_D \cdot x_{R32}^D$  are log transformed and replaced by auxiliary variables, allowing the constraint system to be rewritten in the form given in Eq. 11. Then we solve the KKT system using the Gauss–Newton-type algorithm as given in Algorithm 1. In our implementation, we use

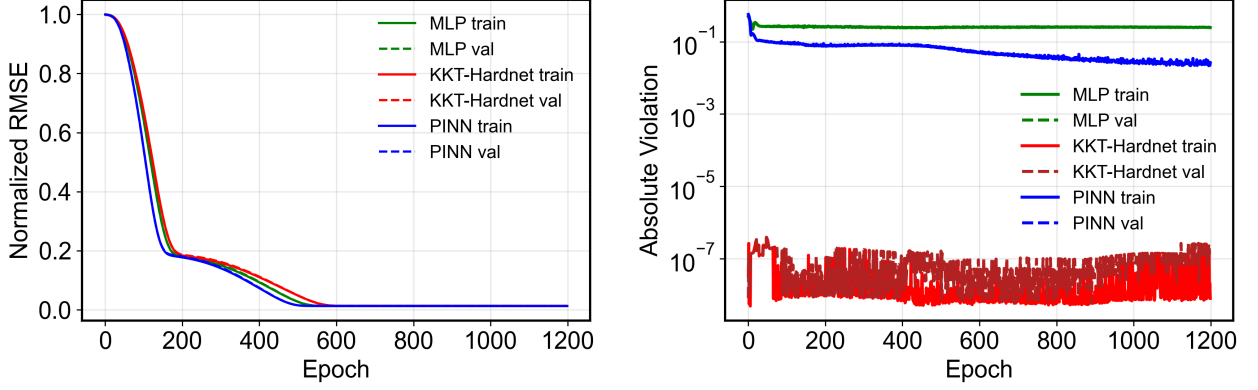


Figure 7: Learning curves for the simulation of extractive distillation-based simulation of R-410A using an ionic liquid [EMIM][SCN]. Left: Normalized RMSE; Right: absolute constraint violation over 1200 epochs.

$K = 30$ ,  $\gamma = 10^{-3}$ , and  $\alpha \in (0, 1]$  is adjusted based on backtracking and Armijo condition. The projection operation is fully differentiable and acts as a corrector layer:  $\mathcal{P}_{\mathcal{S}}(x, \hat{y}_0) = \mathbf{y}^{(K)}$ , where  $\mathcal{S}$  is the feasible manifold defined by the constraints.

We compare the performance of this hard-constrained network (KKT-Hardnet) with a soft penalty-based PINN and an unconstrained MLP, all using identical architectures and optimization settings (learning rate  $10^{-4}$ , 1200 epochs, Adam optimizer). The PINN model includes the six physical constraints as penalty terms in the loss function with a penalty weight  $\omega = 10.0$ . Figure 7 displays the learning curves for normalised RMSE and absolute constraint violation.

Table 4: Model performance comparison on the extractive distillation case study.

Model	Training			Validation		
	MSE	MAPE	$ h $	MSE	MAPE	$ h $
Vanilla MLP	$1.542 \times 10^1$	$8.358 \times 10^8$	$2.48 \times 10^{-1}$	$1.605 \times 10^1$	$8.361 \times 10^8$	$2.49 \times 10^{-1}$
PINN	$1.499 \times 10^1$	$1.308 \times 10^{10}$	$2.61 \times 10^{-2}$	$1.565 \times 10^1$	$1.307 \times 10^{10}$	$2.59 \times 10^{-2}$
KKT-Hardnet	$1.553 \times 10^1$	$5.914 \times 10^9$	$7.90 \times 10^{-9}$	$1.616 \times 10^1$	$5.829 \times 10^9$	$1.26 \times 10^{-7}$

As shown in Table 4, the KKT-Hardnet achieves constraint satisfaction within machine precision ( $\sim 10^{-6}$ ) without requiring any penalty term. Although its MSE is slightly higher than the unconstrained MLP, it eliminates physical inconsistency and constraint violation entirely. In contrast, the PINN, despite a soft penalty, fails to sufficiently reduce constraint violation, indicating that soft regularization alone is insufficient for strict feasibility in this nonlinear, process-driven setting.

### 3.4.3 Analytic projection for affine-in-output constraints

We consider a special case which consists of a subset of four output constraints that are linear in outputs. These include the overall molar balance, the mole fraction balances for distillate and bottoms, and the reflux relation. Specifically:

(C1) Overall molar balance:

$$F_F + F_{IL} = F_D + F_B \quad (57)$$

(C4) Mole fraction closure — Distillate:

$$x_{R32}^D + x_{R125}^D + x_{IL}^D = 1 \quad (58)$$

(C5) Mole fraction closure — Bottoms:

$$x_{R32}^B + x_{R125}^B + x_{IL}^B = 1 \quad (59)$$

(C6) Reflux ratio relation:

$$L = R \cdot F_D \quad (60)$$

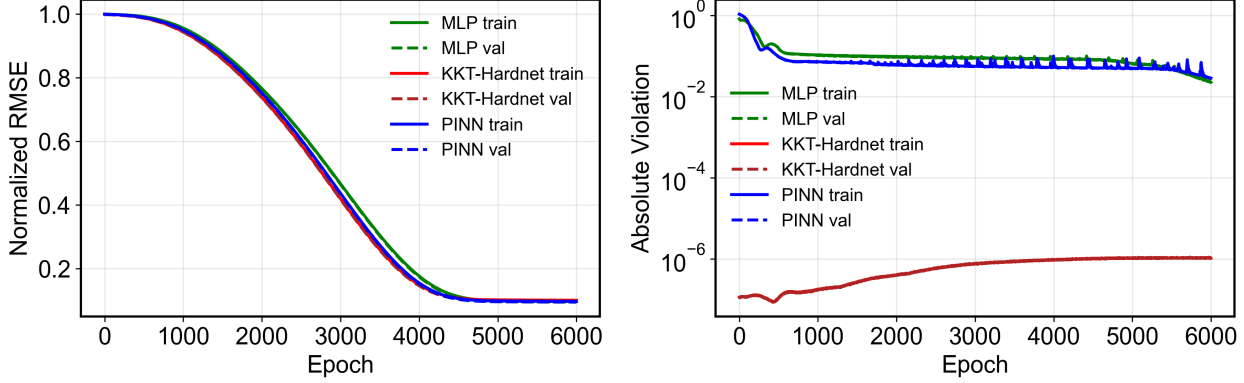


Figure 8: Learning curves for the analytic projection case. Left: Normalized RMSE; Right: absolute constraint violation (log scale).

These constraints define a linear manifold over the 9-dimensional output space. Given a raw neural network prediction  $\hat{\mathbf{y}}_0 \in \mathbb{R}^9$ , we project it onto the feasible manifold using an analytic projection given in Eq. 21:

$$\mathbf{y}_{\text{proj}} = \hat{\mathbf{y}}_0 - \mathbf{B}^\top (\mathbf{B}\mathbf{B}^\top)^{-1} \mathbf{r}, \quad (61)$$

where  $\mathbf{B} \in \mathbb{R}^{4 \times 9}$  encodes the output coefficients of the constraints, and  $\mathbf{r} \in \mathbb{R}^4$  is the residual vector formed from the violation of each constraint. Specifically, for a given input  $\mathbf{x} = (F_F, F_{IL}, R)$ , the residual vector is computed as:

$$\mathbf{r} = \begin{bmatrix} F_F + F_{IL} - (\hat{F}_D + \hat{F}_B) \\ \hat{x}_{R32}^D + \hat{x}_{R125}^D + \hat{x}_{IL}^D - 1 \\ \hat{x}_{R32}^B + \hat{x}_{R125}^B + \hat{x}_{IL}^B - 1 \\ -R \cdot \hat{F}_D + \hat{L} \end{bmatrix} \quad (62)$$

This projection is performed independently for each sample in the batch, and requires no iterative solver or Jacobian computation. The matrix  $\mathbf{B}$  is fixed for each sample based on known input  $\mathbf{x}$ . As such, the projection step is differentiable and computationally efficient.

We compare the analytic projection-based constrained neural network (KKT-Hardnet) with an unconstrained MLP and a soft-constrained PINN, all using identical architectures and training routines. Figure 8 shows the normalized RMSE and constraint violation for all three models. The results in Table 5 clearly show that the analytically projected KKT-Hardnet maintains constraint satisfaction up to numerical precision while achieving comparable MSE and MAPE to the unconstrained MLP. In contrast, the PINN suffers from persistent constraint violations despite soft penalty enforcement.

Table 5: Model performance with analytic projection for output-only linear constraints for the extractive distillation case study.

Model	Training			Validation		
	MSE	MAPE	$ h $	MSE	MAPE	$ h $
MLP	$8.996 \times 10^2$	$2.617 \times 10^8$	$2.25 \times 10^{-2}$	$8.614 \times 10^2$	$2.646 \times 10^8$	$2.25 \times 10^{-2}$
PINN	$9.061 \times 10^2$	$2.533 \times 10^9$	$2.84 \times 10^{-2}$	$8.675 \times 10^2$	$2.485 \times 10^9$	$2.82 \times 10^{-2}$
KKT-Hardnet	$9.752 \times 10^2$	$2.234 \times 10^9$	$1.04 \times 10^{-6}$	$9.336 \times 10^2$	$2.198 \times 10^9$	$1.05 \times 10^{-6}$

This case highlights that when constraints are affine or linear in outputs, an exact and efficient analytic projection can be used to enforce strict feasibility without iterative solvers.

## 4 Conclusions

We have presented a physics-informed neural network architecture that enforces hard nonlinear equality and inequality constraints in both inputs and outputs through a projection layer. By introducing a log-exponential transformation

of general nonlinear equations corresponding to the KKT conditions of the projection, we transform the governing equations to a structured form involving linear and exponential terms. This transformed system of equations is then subjected to a Newton-type iterative scheme, which acts as a differentiable projection layer within the neural network and guarantees constraint satisfaction by solving the KKT conditions. In doing so, we have addressed the limitations of traditional PINNs that rely on soft constraint penalty parameters and lack guaranteed satisfaction of first-principles-based governing equations. Numerical experiments on illustrative examples and a highly nonlinear chemical process simulation problem demonstrate that the proposed approach eliminates constraint violations to within machine precision. It also improves predictive accuracy compared to conventional MLPs and soft-constrained PINNs. Future directions include extending the method for application to differential-algebraic systems, and devising tailored algorithm that exploits the structure and sparsity of the log-exponential system. To improve the initial guess of the Newton step at the projection layer, an unconstrained pre-training phase, followed by the activation of the projection layer may be investigated.

## Acknowledgments

The authors gratefully acknowledge partial funding support from the NSF CAREER award CBET-1943479 and the EPA Project Grant 84097201. Part of the research was conducted with the computing resources provided by Texas A&M High Performance Research Computing.

## References

- [1] George Em Karniadakis, Ioannis G Kevrekidis, Lu Lu, Paris Perdikaris, Sifan Wang, and Liu Yang. Physics-informed machine learning. *Nature Reviews Physics*, 3(6):422–440, 2021.
- [2] Ashfaq Iftakher, Ty Leonard, and M. M Faruque Hasan. Integrating different fidelity models for process optimization: A case of equilibrium and rate-based extractive distillation using ionic liquids. *Computers & Chemical Engineering*, 192:108890, 2025.
- [3] Hamidreza Eivazi, Mojtaba Tahani, Philipp Schlatter, and Ricardo Vinuesa. Physics-informed neural networks for solving reynolds-averaged navier–stokes equations. *Physics of Fluids*, 34(7), 2022.
- [4] Yuntian Chen, Dou Huang, Dongxiao Zhang, Junsheng Zeng, Nanzhe Wang, Haoran Zhang, and Jinyue Yan. Theory-guided hard constraint projection (hcp): A knowledge-based data-driven scientific machine learning method. *Journal of Computational Physics*, 445:110624, 2021.
- [5] Maziar Raissi, Alireza Yazdani, and George Em Karniadakis. Hidden fluid mechanics: Learning velocity and pressure fields from flow visualizations. *Science*, 367(6481):1026–1030, 2020.
- [6] Carlos Sánchez-Sánchez and Dario Izzo. Real-time optimal control via deep neural networks: study on landing problems. *Journal of Guidance, Control, and Dynamics*, 41(5):1122–1135, 2018.
- [7] Pratyush Kumar, James B Rawlings, and Stephen J Wright. Industrial, large-scale model predictive control with structured neural networks. *Computers & chemical engineering*, 150:107291, 2021.
- [8] Atharv Bhosekar and Marianthi Ierapetritou. Advances in surrogate based modeling, feasibility analysis, and optimization: A review. *Computers & Chemical Engineering*, 108:250–267, 2018.
- [9] Ashfaq Iftakher, Chinmay M Aras, Mohammed Sadaf Monjur, and M. M. Faruque Hasan. Data-driven approximation of thermodynamic phase equilibria. *AIChE Journal*, 68(6):e17624, 2022.
- [10] Ashfaq Iftakher, Chinmay M Aras, Mohammed Sadaf Monjur, and M. M. Faruque Hasan. Guaranteed error-bounded surrogate modeling and application to thermodynamics. In *Computer Aided Chemical Engineering*, volume 49, pages 1831–1836. Elsevier, 2022.
- [11] Kevin McBride and Kai Sundmacher. Overview of surrogate modeling in chemical process engineering. *Chemie Ingenieur Technik*, 91(3):228–239, 2019.
- [12] Ruth Misener and Lorenz Biegler. Formulating data-driven surrogate models for process optimization. *Computers & Chemical Engineering*, 179:108411, 2023.
- [13] Zachary T Wilson and Nikolaos V Sahinidis. The alamo approach to machine learning. *Computers & Chemical Engineering*, 106:785–795, 2017.
- [14] Alison Cozad, Nikolaos V Sahinidis, and David C Miller. Learning surrogate models for simulation-based optimization. *AIChE Journal*, 60(6):2211–2227, 2014.
- [15] Kurt Hornik, Maxwell Stinchcombe, and Halbert White. Multilayer feedforward networks are universal approximators. *Neural networks*, 2(5):359–366, 1989.

- [16] Alex Krizhevsky, Ilya Sutskever, and Geoffrey E Hinton. Imagenet classification with deep convolutional neural networks. *Communications of the ACM*, 60(6):84–90, 2017.
- [17] Ian Goodfellow, Jean Pouget-Abadie, Mehdi Mirza, Bing Xu, David Warde-Farley, Sherjil Ozair, Aaron Courville, and Yoshua Bengio. Generative adversarial networks. *Communications of the ACM*, 63(11):139–144, 2020.
- [18] Yann LeCun, Yoshua Bengio, and Geoffrey Hinton. Deep learning. *nature*, 521(7553):436–444, 2015.
- [19] Ashish Vaswani, Noam Shazeer, Niki Parmar, Jakob Uszkoreit, Llion Jones, Aidan N Gomez, Łukasz Kaiser, and Illia Polosukhin. Attention is all you need. *Advances in neural information processing systems*, 30, 2017.
- [20] Yi Ming Ren, Mohammed S Alhajeri, Junwei Luo, Scarlett Chen, Fahim Abdullah, Zhe Wu, and Panagiotis D Christofides. A tutorial review of neural network modeling approaches for model predictive control. *Computers & Chemical Engineering*, 165:107956, 2022.
- [21] Shengze Cai, Zhiping Mao, Zhicheng Wang, Minglang Yin, and George Em Karniadakis. Physics-informed neural networks (pinns) for fluid mechanics: A review. *Acta Mechanica Sinica*, 37(12):1727–1738, 2021.
- [22] Ashfaq Iftakher, Mohammed Sadaf Monjur, Ty Leonard, Rafiqul Gani, and MM Faruque Hasan. Multiscale high-throughput screening of ionic liquid solvents for mixed-refrigerant separation. *Computers & Chemical Engineering*, 199:109138, 2025.
- [23] Karthik Kashinath, M Mustafa, Adrian Albert, JL Wu, C Jiang, Soheil Esmailzadeh, Kamyar Azizzadenesheli, R Wang, Ashesh Chattopadhyay, A Singh, et al. Physics-informed machine learning: case studies for weather and climate modelling. *Philosophical Transactions of the Royal Society A*, 379(2194):20200093, 2021.
- [24] Maziar Raissi, Paris Perdikaris, and George E Karniadakis. Physics-informed neural networks: A deep learning framework for solving forward and inverse problems involving nonlinear partial differential equations. *Journal of Computational physics*, 378:686–707, 2019.
- [25] Shengze Cai, Zhicheng Wang, Sifan Wang, Paris Perdikaris, and George Em Karniadakis. Physics-informed neural networks for heat transfer problems. *Journal of Heat Transfer*, 143(6):060801, 2021.
- [26] Hao Chen, Gonzalo E Constante Flores, and Can Li. Physics-informed neural networks with hard linear equality constraints. *Computers & Chemical Engineering*, 189:108764, 2024.
- [27] Sifan Wang, Xinling Yu, and Paris Perdikaris. When and why pinns fail to train: A neural tangent kernel perspective. *Journal of Computational Physics*, 449:110768, 2022.
- [28] Kaiwen Ma, Nikolaos V Sahinidis, Satyajith Amaran, Rahul Bindlish, Scott J Bury, Devin Griffith, and Sreekanth Rajagopalan. Data-driven strategies for optimization of integrated chemical plants. *Computers & Chemical Engineering*, 166:107961, 2022.
- [29] Aditi Krishnapriyan, Amir Gholami, Shandian Zhe, Robert Kirby, and Michael W Mahoney. Characterizing possible failure modes in physics-informed neural networks. *Advances in neural information processing systems*, 34:26548–26560, 2021.
- [30] Chuwei Wang, Shanda Li, Di He, and Liwei Wang. Is  $L^2$  physics-informed loss always suitable for training physics-informed neural networks? *Advances in Neural Information Processing Systems*, 35:8278–8290, 2022.
- [31] Pratik Rathore, Weimu Lei, Zachary Frangella, Lu Lu, and Madeleine Udell. Challenges in training pinns: A loss landscape perspective. *arXiv preprint arXiv:2402.01868*, 2024.
- [32] Youngjae Min, Anoopkumar Sonar, and Navid Azizan. Hard-constrained neural networks with universal approximation guarantees. *arXiv preprint arXiv:2410.10807*, 2024.
- [33] Pablo Márquez-Neila, Mathieu Salzmann, and Pascal Fua. Imposing hard constraints on deep networks: Promises and limitations. *arXiv preprint arXiv:1706.02025*, 2017.
- [34] Tom Beucler, Michael Pritchard, Stephan Rasp, Jordan Ott, Pierre Baldi, and Pierre Gentine. Enforcing analytic constraints in neural networks emulating physical systems. *Physical review letters*, 126(9):098302, 2021.
- [35] Priya L Donti, David Rolnick, and J Zico Kolter. Dc3: A learning method for optimization with hard constraints. *arXiv preprint arXiv:2104.12225*, 2021.
- [36] Jorge Nocedal and Stephen J Wright. *Numerical optimization*. Springer, 1999.
- [37] Brandon Amos and J Zico Kolter. Optnet: Differentiable optimization as a layer in neural networks. In *International conference on machine learning*, pages 136–145. PMLR, 2017.
- [38] Akshay Agrawal, Brandon Amos, Shane Barratt, Stephen Boyd, Steven Diamond, and J Zico Kolter. Differentiable convex optimization layers. *Advances in neural information processing systems*, 32, 2019.

- [39] Giacomo Lastrucci and Artur M Schweidtmann. Enforce: Exact nonlinear constrained learning with adaptive-depth neural projection. *arXiv preprint arXiv:2502.06774*, 2025.
- [40] Houyuan Jiang. Smoothed fischer-burmeister equation methods for the complementarity problem. *Department of Mathematics, The University of Melbourne (Australia)*, 1997.
- [41] A Paszke. Pytorch: An imperative style, high-performance deep learning library. *arXiv preprint arXiv:1912.01703*, 2019.
- [42] Diederik P Kingma. Adam: A method for stochastic optimization. *arXiv preprint arXiv:1412.6980*, 2014.
- [43] João Carlos Alves Barata and Mahir Saleh Hussein. The moore–penrose pseudoinverse: A tutorial review of the theory. *Brazilian Journal of Physics*, 42:146–165, 2012.
- [44] Mohammed Sadaf Monjur, Ashfaq Iftakher, and M. M. Faruque Hasan. Separation process synthesis for high-gwp refrigerant mixtures: Extractive distillation using ionic liquids. *Industrial & Engineering Chemistry Research*, 61(12):4390–4406, 2022.